

Force distributions in a triangular lattice of rigid bars

Brian P. Tighe and Joshua E. S. Socolar

*Department of Physics and Center for Nonlinear and Complex Systems,
Duke University, Durham, NC 27708*

David G. Schaeffer, W. Garrett Mitchener, and Mark L. Huber

*Department of Mathematics and Center for Nonlinear and Complex Systems,
Duke University, Durham, NC 27708*

(Dated: December 2, 2024)

We study the uniformly weighted ensemble of force balanced configurations on a triangular network of nontensile contact forces. For periodic boundary conditions corresponding to isotropic compressive stress, we find that the probability distribution for single-contact forces decays faster than exponentially. This super-exponential decay persists in lattices diluted to the rigidity percolation threshold. On the other hand, for anisotropic imposed stresses, a broader tail emerges in the force distribution, becoming a pure exponential in the limit of infinite lattice size and infinitely strong anisotropy.

PACS numbers: 45.70.-n, 46.65.+g, 05.40.-a, 83.80.Fg

I. INTRODUCTION

Materials composed of hard cohesionless grains, such as dry sand, exhibit many remarkable properties ranging from cluster formation in gaseous phases,[1, 2, 3] to unexpected flows and jets in fluid-like phases,[4, 5] and to complex organization of inhomogeneous stresses in dense fluid or solid phases.[6, 7, 8] In this paper we focus on one feature of the solid phase that has received much attention: the distribution $P(f)$ of contact forces between grains in a system that is supporting a macroscopic compression or shear force. In a number of experiments and numerical simulations involving non-cohesive grains, $P(f)$ appears to decay approximately exponentially at large f ,[9, 10, 11, 12] which runs counter to the naïve expectation of a Gaussian distribution about some average f . Several theoretical analyses of model systems have indicated possible explanations for the exponential tail,[13, 14, 15, 16, 17] including an analytic calculation for a special case of isostatic packings of frictionless disks. [18] Still, a fundamental understanding of the phenomenon has not been achieved.

To motivate the problem we consider, we recall that for generic packings of frictional and/or nonspherical hard particles geometrical constraints permit the formation of more contacts than would be required for supporting imposed stresses. That is, the contact network can contain enough contacts that the stress balance conditions do not determine a unique configuration of the intergrain forces. In such cases, the determination of $P(f)$ must involve some sort of average over the ensemble of possible force configurations. It has been suggested by Edwards that the appropriate measure in configuration space for this ensemble is a flat one; i.e., that all possible force configurations should be considered equally weighted.[19]

In this paper we investigate in one context the question of whether Edwards' hypothesis leads to exponential tails in $P(f)$ for non-cohesive grains of a system in which

the contact network forms a triangular lattice. We first study the case of hydrostatic compression, where our results confirm those of Snoeijer et al,[14, 15] though we employ different boundary conditions and different numerical methods. We then examine the effects of diluting the lattice to the rigidity percolation threshold. The transition appears to be first order, with a finite jump in the number of available configurations at threshold. $P(f)$ becomes substantially broader than in the full lattice case, but still decays faster than exponentially on the lattice sizes within our numerical reach. Finally, we consider the effects of anisotropic imposed stresses. We show that strong anisotropy must produce an exponential tail in large systems and present numerical results showing the approach to this limit for varying degrees of anisotropy. We suggest that anisotropy plays an important role in experiments in which $P(f)$ is measured.

In the model described below, all forces are directed along the line of contact between two grains and tensile forces are not allowed. This may be thought of as corresponding to the case of frictionless, non-cohesive, circular disks, though a generic set of perfectly circular disks could not form as many contacts as are present in the model. Periodic boundary conditions are imposed, so there is no distinction between bulk and boundary contacts. By treating the force network without regard to any distortions of the lattice, we are considering systems of grains with elastic moduli large enough that the boundary forces cause negligible strain; i.e., we consider either very hard grains or very weak boundary forces. In all cases, we fix the contact network and study the ensemble of force configurations on that network. We note that fluctuations are large. $P(f)$ in any given force configuration may look quite different from the $P(f)$ obtained by averaging over configurations, even on the largest lattices we have studied.

For the smallest nontrivial lattice, consisting of nine grains, we calculate $P(f)$ both analytically and numerically.

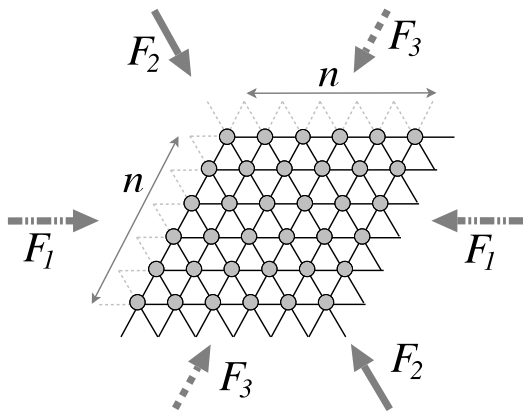


FIG. 1: An $n \times n$ triangular lattice (with $n = 6$). Under periodic boundary conditions light edges on the left are identified with dangling edges on the right and light edges on top are identified with dangling edges on the bottom. The macroscopic stress state is fixed by imposing compressive forces F_1 , F_2 , and F_3 along each lattice direction.

ically, and find good agreement. For larger lattices, we employ numerical sampling methods involving Monte Carlo moves that maintain the force balance constraints at all times (in contrast to simulated annealing methods [14, 15, 20]).

II. THE LATTICE

We study the distribution of bond strengths on an $n \times n$ triangular lattice corresponding to the contacts in a hexagonal packing of monodisperse circular grains. We consider a system in the shape of a rhombus, having n^2 bonds or edges in each lattice direction, and subject to periodic boundary conditions, as illustrated in Fig. 1. Each edge carries a scalar variable f specifying the magnitude of the force transmitted across a contact. In order to fix the three components of the macroscopic stress tensor σ_{ij} we specify the total compressive forces F_1 , F_2 , and F_3 supported along each of the three lattice directions.

There are $3n^2$ variables in the system. For each grain, the vector force balance condition imposes 2 constraints. These constraints are not all independent, however. The periodic boundary conditions guarantee that the sum of all the single-grain constraint equations is trivially zero, leaving $2n^2 - 2$ independent constraints. Fixing F_1 , F_2 , and F_3 imposes 3 additional constraints, for a total of $2n^2 + 1$ constraints. This leaves $n^2 - 1$ degrees of freedom in the force configuration.

In addition to force balance equations, there are inequality constraints associated with the fact that the material is non-cohesive. No force f is allowed to be negative. It is this condition that introduces nonlinearity in the system. For any two force balanced, tension free configurations on the lattice, any weighted average with positive weights will also be force balanced and tension free. Sums with a negative weighting of a configuration, however, will not always be allowed, as they may contain negative forces on some edges.

We represent the system configuration by a vector of forces f_i , $i = 1 \dots 3n^2$. The above constraints create a space of possible configurations that fills a finite, convex $n^2 - 1$ -dimensional volume, with boundaries determined by the inequalities $f_i \geq 0$. Our interpretation of the Edwards hypothesis is to assign a uniform probability (Lebesgue) measure on the space of allowed configurations.

III. ISOTROPIC LATTICE

In principle, $P(f)$ can be calculated in the following way. Fix one edge to carry force f ; this restricts the system to a $(n^2 - 2)$ -dimensional subset of the $(n^2 - 1)$ -dimensional allowed volume V in configuration space. $P(f)$ is simply the ratio of the $(n^2 - 2)$ -dimensional “area” to the $(n^2 - 1)$ -dimensional total volume. More formally, let E_m be the set of 6 edges touching node m ; let $\hat{e}_g^{(m)}$, $g = 1 \dots 6$, be a unit vector along edge g in E_m pointing towards node m ; and let L_k , $k = 1 \dots 3$, be the set of n^2 edges along lattice direction k . Then we have

$$P(f) = \frac{1}{V} \int_{\{f_j \geq 0\}} \left(\prod_{j=1}^{3n^2} df_j \right) \delta(f_i - f) \left[\prod_{m=1}^{n^2} \delta \left(\sum_{f_g \in E_m} f_g \hat{e}_g^{(m)} \right) \right] \left[\prod_{k=1}^3 \delta \left(nF_k - \sum_{f_l \in L_k} f_l \right) \right] \quad (1)$$

where edge i has been fixed to have value f . The integral is taken over all f 's. The first delta function ensures that edge i carries force f . The next ensures force balance at each vertex, and the last enforces the boundary conditions. The integral represents the volume of a $(n^2 - 2)$ -dimensional slice of a polytope, therefore $P(f)$

on an $n \times n$ lattice is a piecewise polynomial of order $n^2 - 2$.

The average force on the edges in L_k is F_k/n . The last factor in 1 requires comment. For definiteness, consider $k = 2$. Let us divide the set of edges in L_2 into n layers, each layer containing the n edges that intersect a line

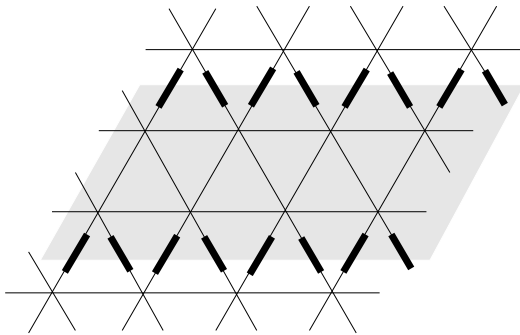


FIG. 2: A slab of material and set of edges used to prove that each layer of edges in L_k must have a sum of forces equal to F_k .

along one of the other edge directions. The following argument shows that the sum of the f_j on each layer must be equal to F_2 . Fig. 2 shows a shaded slab of the system. The total force on this slab must be zero, which implies that the vector sum of the forces on the edges indicated by thick lines on one side of the slab must be equal to the vector sum of the forces on the other side. Since the vector sum has a unique decomposition into contributions from the L_2 edges and the L_3 edges, the sum of the f_j 's in each direction must independently be the same on both sides of the slab. This argument is independent of the thickness of the slab, so in the L_2 direction each of the n layers must have f_j 's that sum to F_2 , and similarly for L_1 and L_3 .

For the 3×3 case, the integral can be evaluated analytically. Here we state the isotropic result; the anisotropic result is presented below. The calculation is detailed in Appendix A. (We have not found an analytic expression for $P(f)$ for arbitrary lattice size. See Ref. [15], however, for a treatment of the case in which the sum $F_1 + F_2 + F_3$ is fixed, but not the individual F_k .) In the isotropic case ($F_1 = F_2 = F_3 = F$), we find

$$P(f) = \frac{8}{45F^8} \Theta(f) \Theta(F-f) (F-f)^2 \quad (2)$$

$$\times (5F^5 + 73fF^4 - 111f^2F^3 + 125f^3F^2 - 59f^4F + 9f^5)$$

where $\Theta(f)$ is the Heaviside step function. This expression is plotted in Fig. 5

On larger lattices we employ numerical methods to measure $P(f)$. This requires generating numerous configurations in the allowed volume of configuration space in a manner consistent with the Edwards flat measure. Previous work has implemented a simulated annealing algorithm, which generates each configuration by starting from a random point in the space of all possible f_i and relaxing to some point in the lower dimensional subset of interest.[14, 15] We employ a different technique in which, starting from one force-balanced configuration – a point in the allowed subset of stress states – new configurations are generated via moves that always produce allowed configurations. By identifying a set of moves that

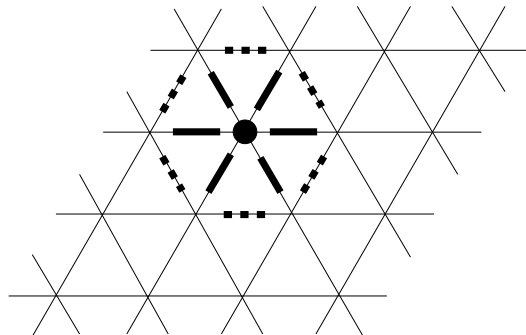


FIG. 3: The wheel move associated with the node marked by a disk. Forces are shifted by an amount Δf , chosen to be small enough that no edge becomes negative. Force on each edge marked with a thick solid segment is increased and on each edge marked with a thick dashed segment is decreased, or vice versa.

span this compact space, reach any set of positive volume in a finite time, and involve symmetric transition probabilities, we can be sure that at sufficiently long times the space is being sampled with uniform measure.[21] These moves are described below.

For the $n \times n$ lattice with $n \geq 3$, we construct a set of n^2 *wheel moves*, one centered on each node. The wheel move associated with a given node acts on the nearest neighbor edges (“spokes”) and next nearest neighbor edges (“rim”) of the node, reducing one set of f 's and augmenting the other by the same amount. The move is implemented in the following steps. Identify the smallest force on the spokes and call it s_{min} ; likewise, call the smallest force on the rim r_{min} . Randomly choose a force increment Δf with uniform measure on the interval $[-s_{min}, r_{min}]$. Adding Δf to every edge on the spokes and subtracting it from every edge on the rim, which respects force balance on every node touching the wheel, constitutes a wheel move.

In the space of linear combinations of wheel moves, there is exactly one null direction; i.e., there is one linear combination of wheel moves, up to an overall multiplicative factor, that results in no change to any edge of the lattice. Thus the number of linearly independent wheel moves is $n^2 - 1$, which is exactly the number required to span the space of force configurations. This is proven in Appendix B.

Fig. 4 illustrates a geometric subtlety that must be taken into account when attempting to explore the allowed stress states using wheel moves (or any other basis set of moves). Since the given pair of basis vectors span the two-dimensional convex space shown, it is clearly possible to navigate from any interior point to any other by making discrete steps along the basis vectors. It may not be possible, however, to make a move in either basis direction if the initial configuration lies exactly on a corner. In higher dimensions it is likewise possible to be stuck on a corner or a boundary of higher dimension. It is therefore important to find initial configurations that lie in

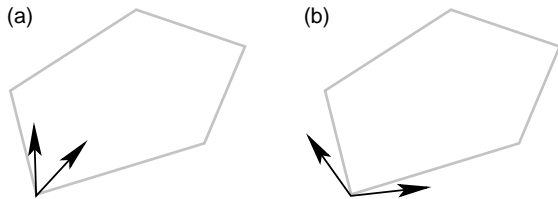


FIG. 4: A two-dimensional convex space, outlined in gray, with two different sets of basis vectors. The basis in (a) is such that it is possible to move off the lower-lefthand corner along either basis direction, while in (b) this is not the case.

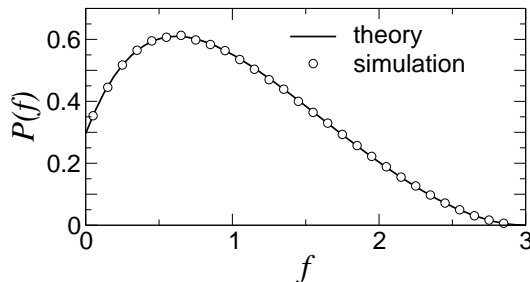


FIG. 5: 3×3 triangular lattice under isotropic stress. The curve gives the force distribution, points represent numerical simulations of the same quantity. $P(f)$ vanishes at F , the force imposed along each lattice direction. Here $F = 3$, fixing $\langle f \rangle = 1$.

the interior of the space, rather than on a boundary, for the purposes of our Monte Carlo sampling technique. An algorithm such as the one described above, beginning at an interior point, can come arbitrarily close to all boundaries but will never reach them. Regions near corners are visited infrequently but for long times in such a way that, for sufficiently long runtime, the space is sampled with uniform measure. [21]

Fig. 5 shows the agreement between the exact calculation and simulation on the 3×3 lattice. The forces are normalized by choosing F such that the average force $\langle f \rangle$ is unity. The peak near $\langle f \rangle$ is typical for larger lattices as well, but finite size effects are clearly evident in the tail, since $P(f)$ must go to zero at $f = F$ (here $F = 3$).

A typical configuration for the 15×15 lattice is shown in Fig. 6. $P(f)$'s for the cases $n = 5, 10, 15$, and 20 are shown in Fig. 7. The peak near $\langle f \rangle$ is again apparent, and for small f the curves appear to coincide, though small differences exist that are masked by the logarithmic scale. For $f \gtrsim 3\langle f \rangle$ the curves separate, with the $n = 5$ distribution decaying most rapidly. The four distributions in the figure all decay faster than exponentially, and they broaden slightly with increasing n .

To gain confidence that the curves are converging to a large system limit, we measured correlations between forces as a function of the distance between edges. In directions both longitudinal and transverse to a particular edge, as shown in Fig. 8, we see that on a 20×20 lattice correlations have decayed to the 1% level at a distance of

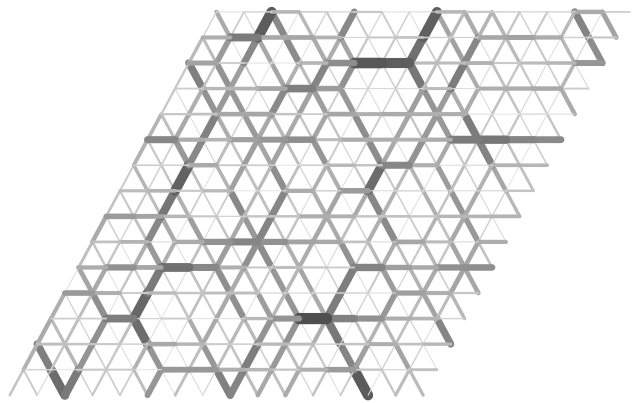


FIG. 6: A typical 15×15 lattice. The force on an edge is redundantly mapped to color and width (stronger forces are darker and thicker).

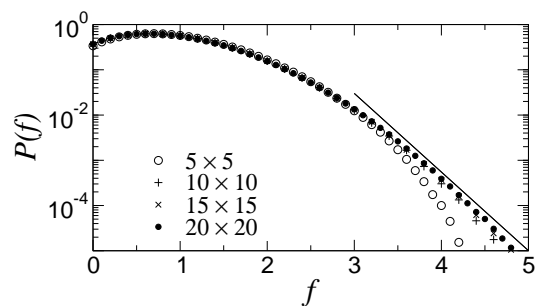


FIG. 7: Force distributions for $n \times n$ lattices under isotropic stress for $n = 5, 10, 15$, and 20 . For all cases the decay is faster than exponential. The $n = 15$ and $n = 20$ cases are nearly identical, indicating convergence to a universal curve for large systems. The straight line is drawn as a guide to the eye. For each curve, $\langle f \rangle = 1$.

10 lattice constants. On larger lattices we see exponential decay with a decay length of approximately 3 lattice constants, although much more data on larger lattices would be necessary to measure this precisely. We therefore expect to see little difference in $P(f)$ for lattices larger than $n = 20$. Supporting this expectation, there is very little difference between the $n = 15$ and $n = 20$ distributions for f up to the largest values we have measured, which covers five decades of P . Though it is conceivable that the asymptotic form of $P(f)$ at large f in our model is exponential, the domain displayed in Fig. 7 is the relevant one for comparison with experiments, and it clearly shows a decay that is faster than exponential.

IV. DILUTED LATTICE

Real disks are not perfectly monodisperse, so in any hexagonal packing of hard disks some of the bonds on the triangular lattice will not actually be present. For a given stress state, a diluted lattice has fewer bonds to carry the same force. Those remaining will, on average, carry more

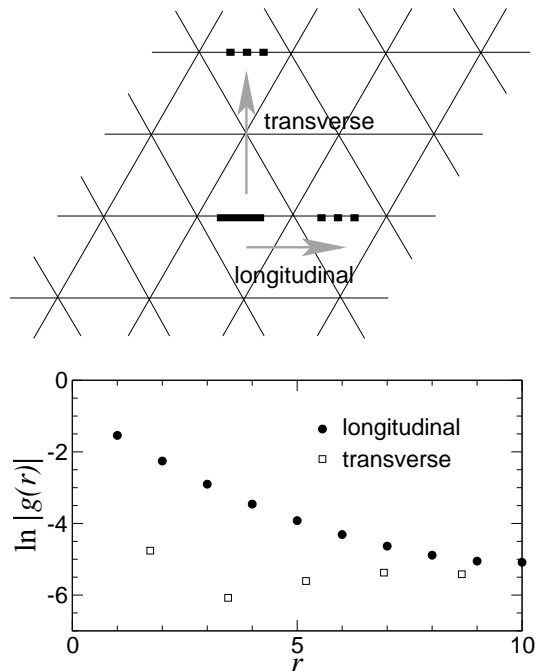


FIG. 8: Above, correlations are calculated in the longitudinal and transverse directions. Below, correlation function $g(r) = \langle f_i f_{i+r} \rangle - \langle f_i^2 \rangle$ on a 20×20 lattice. The correlation is computed for edges that have the same orientation. The longitudinal correlation refers to displacements by r lattice constants along the direction of the edge. The transverse correlation refers to displacements perpendicular to the edge. The plots above are averaged over multiple reference edges. The transverse correlations are in fact negative, but we take their absolute value to facilitate plotting on a log scale.

force, resulting in a broadening of the tail of $P(f)$. As the number of edges removed from the lattice increases, the force configurations tend to become less homogeneous, with strong forces concentrated in chain-like structures. As more edges are deleted there comes a point where the lattice can no longer support the imposed stress; this is the rigidity-percolation transition. Fig. 9 shows a typical force configuration for a randomly diluted lattice. We study randomly diluted lattices at the transition to see whether the broadening takes the form of an exponential decay.

The random dilution process merits further remark. For a random process in which each bond is removed with probability ϕ , the infinite triangular lattice under isotropic compression cannot support stress for any $\phi > 0$. [22] Thus in an $n \times n$ simulation the fraction (not the number n_d) of deleted edges at the rigidity percolation threshold goes to zero as $n \rightarrow \infty$. As an arbitrarily large real hexagonal packing does support compression, this suggests that the process of bond breaking in the real packing does not happen randomly but rather in a correlated way. Nevertheless, our simulations employ random dilution on finite lattices.

We construct lattices at the rigidity percolation thresh-

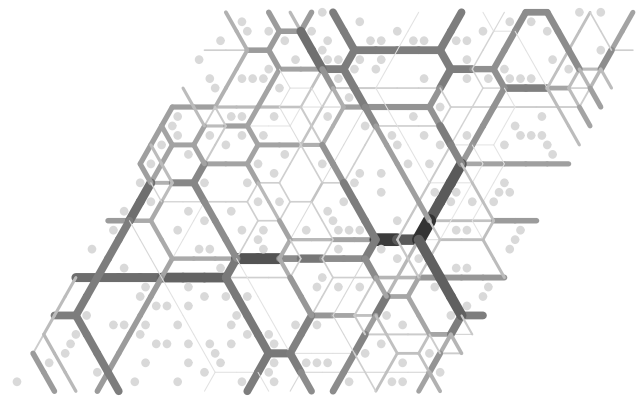


FIG. 9: A 15×15 lattice at rigidity percolation. Deleted edges are covered with disks. The force on an edge is redundantly mapped to color and width (stronger forces are darker and thicker).

old in the following way. Given the imposed macroscopic stress and beginning with an empty lattice, edges are selected at random to be added to the lattice. After each addition, we check to see if the lattice is capable of supporting the imposed stress using the simplex algorithm.[23] We take the lattice to be at threshold when it first supports the imposed stress, at which point we know that there exists at least one edge such that, when removed, the system could no longer support the stress. The edges that have *not* been added to the lattice at this stage are called “deleted edges.” Our construction yields a lattice in which deletions are randomly distributed in space. Note that the process will in general yield some edges that are present but not connected to the edge network in a way that allows them to bear any force. We refer to these edges as “effectively deleted.”

These effectively deleted edges on a lattice supporting compressive forces can be identified in the following way. Consider the 6 edges that meet at a given node. An edge becomes effectively deleted if its opposite edge has been deleted (possibly effectively) and at least one of the edges making a 120° angle with it has also been deleted (possibly effectively). Under these conditions any force on the edge in question can not be balanced by positive forces on the other edges sharing the node. To find all of the effectively deleted edges we examine all nodes repeatedly until no new deletions are found.

The wheel moves used for investigation of the undiluted lattice no longer work on the diluted lattice. The wheel moves add or subtract a quantity Δf to each edge they touch, but this is impossible if one of the edges is deleted. Therefore each deleted edge renders unusable the four wheel moves to which it belongs. To salvage a set of moves that span the appropriate space, linear combinations of the wheel moves can be formed that leave the deleted edge unaffected. For a single deleted edge there are three linearly independent combinations of the four wheel moves that edge touches which preserve

the deleted edge. The deletion has reduced the available degrees of freedom by one when many edges have been deleted. More complicated linear combinations of wheel moves can be found that preserve the vanishing force on all deleted and effectively deleted edges.

We refer to a particular linear combination of wheel moves that remains a viable move on a diluted lattice as a “multi-wheel move.” Let the number of linearly independent multi-wheel moves be N_m . Just as the undiluted lattice had n^2 wheel moves and $n^2 - 1$ degrees of freedom, the diluted lattice having N_m multi-wheel moves has $N_m - 1$ degrees of freedom. Finding a complete set of multi-wheel moves then provides not only a means to perform numerical simulation but also a count of the degrees of freedom in the diluted system.

A linearly independent set of N_m multi-wheel moves on the diluted lattice can be constructed as follows. For $j = 1 \dots n^2$, form a vector $\vec{w}_j \in \mathbf{R}^{n_d}$ such that the components of \vec{w}_j specify the effect of the wheel move centered on node j on the *deleted* edges. That is, $(\vec{w}_j)_i = +1$ if the i^{th} deleted edge is a spoke of node j , -1 if the i^{th} deleted edge is a rim of node j , and 0 otherwise. Form the $n_d \times n^2$ matrix $W_{ij} = (\vec{w}_j)_i$. Consider a linear combination of wheel moves with coefficients m_k , $k = 1 \dots n^2$. This linear combination has no effect on deleted edges if and only if $W\vec{m} = 0$. Thus $N_m = \dim N(W) = n^2 - \text{rank}(W)$, where $N(W)$ is the null space of W .

Note that we demand the wheel moves respect both real and effective deletions. Were we not to specify effective deletions as well, the algorithm would in general produce additional multi-wheel moves which were nonzero on some effectively deleted edges. This is because the multi-wheel moves could also act on a lattice that supports tensile as well as compressive forces. On such a lattice there are fewer effective deletions; in particular, a node could be force-balanced having only three edges all on the same side of a line through the node. To model a noncohesive material, then, we must include these additional effective deletions as well.

We use the following technique to investigate the degrees of freedom in lattices at threshold. Edges are added to a lattice one at a time until the rigidity percolation threshold is reached, the set of wheel moves on that threshold lattice are constructed to determine the dimension of the volume of allowed configurations in state space $N_m - 1$, and the process is repeated for a number of threshold lattices. We refer to the system as having $N_m - 1$ degrees of freedom, as this is the number of multi-wheel moves it possesses. These lattices have differing numbers of deleted edges. For lattice with the *same* number of deleted edges n_d we calculate the average ratio of the number of degrees of freedom of the dilute system to the number in an undiluted one: $\langle \delta \rangle = (\langle N_m \rangle - 1)/(n^2 - 1)$. Figure 10 shows $\langle \delta \rangle$ plotted against the fraction of deleted edges $\phi = n_d/3n^2$. A discrete jump in $\langle \delta \rangle$ emerges as ϕ is decreased for systems larger than 15×15 , indicating that the transition is first order. This suggests that $P(f)$ near the transition

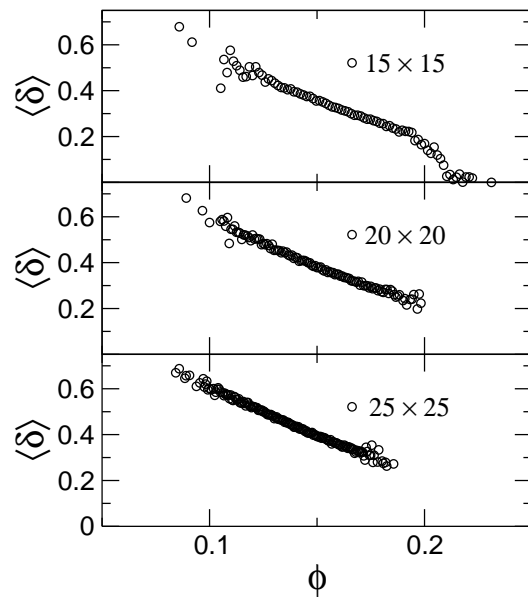


FIG. 10: The ratio of average number of degrees of freedom in threshold lattices to the number in the undiluted case $\langle \delta \rangle = (\langle N_m \rangle - 1)/(n^2 - 1)$ vs. the ratio of deleted edges in the threshold lattice to the total number of edges $\phi = n_d/3n^2$. For each plot a number of lattices at the rigidity-percolation threshold were generated and the degrees of freedom and deleted edges counted. For large enough lattices, the system has a large number of degrees of freedom available as soon as rigidity-percolation is reached. Note that the observed interval of ϕ values shifts as the lattice size is increased.

point is unlikely to show qualitatively different behavior from that of the undiluted lattice, though a quantitative broadening of the force distribution is expected.

We measure $P(f)$ averaged over a number of threshold 20×20 lattices. The resulting distribution is indeed much broader than the undiluted case, but there is still curvature in the distribution on a linear-log plot. Numerical studies in this regime are hampered by two factors. First, each multi-wheel move requires the examination of many edges to ensure that no f_j becomes negative. Second, the maximum size of a multi-wheel move is typically quite small because the move touches several edges that carry small forces. The volume that we are attempting to sample with uniform measure is still convex but contains many corners that are not easily accessed. The data obtained for a given lattice may exhibit a bias depending on the initial configuration unless the number of moves considered is extremely large.

We have gathered data using two procedures. In one case we construct a large number of threshold lattices, find a single initial configuration for each and collect force data from 5×10^4 wheel moves, then average all of the data together to determine $P(f)$ averaged over lattices. To find initial configurations we use the simplex method several times with different coefficients and average the results, thereby avoiding configurations that lie on the boundary of the allowed volume. We cannot be sure,

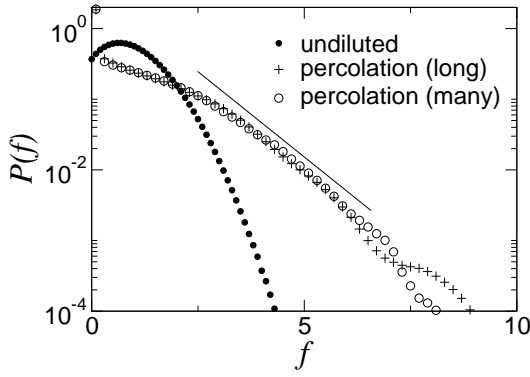


FIG. 11: $P(f)$ for 20×20 triangular lattices diluted to the rigidity-percolation threshold. The plus signs represent an average over 2.5×10^6 moves on a single randomly diluted lattice. The open circles represent an average over 75 lattices, each run for 5×10^4 moves. The straight line is a guide to the eye.

however, that this method is free of systematic bias. In the second case, we consider a single lattice at threshold (with a typical number of degrees of freedom), find 25 different initial configurations and run 2.5×10^6 multi-wheel moves from each one, averaging the force data to obtain the $P(f)$ associated with that particular lattice. The results are shown in Fig. 11. As may be expected given the first-order nature of the rigidity percolation transition, neither procedure produces an exponential tail in P at large f . We conclude that random dilution to the rigidity percolation threshold does not produce exponential tails for triangular lattices.

V. ANISOTROPIC LATTICE

We now consider the *undiluted* lattice with anisotropic stresses imposed by choosing F_1 different from F_2 and F_3 . For example, one lattice direction may be subject to stronger compression than the others, creating qualitatively distinct force distributions in the strong and weak directions. We will show that in strongly anisotropic systems the strong direction contributes an exponential decay to the tail of $P(f)$.

We consider $F_1 = F + \Delta$, $F_2 = F_3 = F$, and parameterize the anisotropy by $\alpha = (F + \Delta)/F$, so that $\alpha = 1$ corresponds to isotropic stress. In terms of $\langle f \rangle$, $F = 3n\langle f \rangle/(2 + \alpha)$. The average force in the weak direction $\langle f_w \rangle = F/n$, while that in the strong direction is $\langle f_s \rangle = (F + \Delta)/n$. Similarly, forces in the weak direction can not exceed F , and those in the strong direction can not exceed $F + \Delta$. Forces in the strong direction will populate the tail of $P(f)$.

In the limit $\alpha \rightarrow \infty$ the system becomes much simpler: only the strong direction carries force, doing so via n chains of n edges, each edge in a given chain carrying the same force as shown in Fig. 12. The forces on the n chains must sum to Δ .

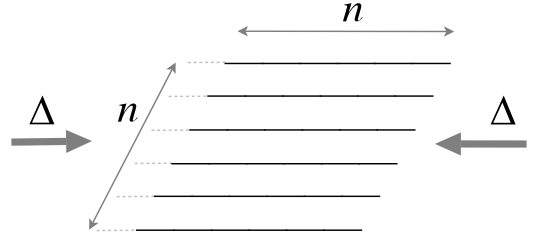


FIG. 12: $\alpha \rightarrow \infty$ limit of the $n \times n$ triangular lattice. Dashed edges represent attachments under periodic boundary conditions. The macroscopic stress state is fixed by imposing compressive force Δ along the strong lattice direction, the only one carrying force. Force is transmitted along n chains, each composed of n edges, in any way such that a sum over chains yields Δ and all forces remain compressive.

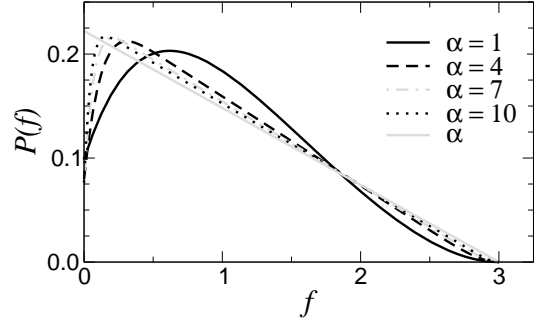


FIG. 13: 3×3 triangular lattice under anisotropic stress. The force distribution $P_s(f)$ for forces in the strong direction is plotted for increasing anisotropy. Each distribution is scaled to $\langle f_s \rangle = 1$. The limiting form is a piecewise linear function of f . P_s for finite anisotropy has a linear region in the middle; this region grows in width and approaches the limiting slope as anisotropy is increased.

Simple dimensional analysis of the scaling of the allowed volume when one chain is fixed at force f yields

$$\lim_{n \rightarrow \infty} P(f) \propto \lim_{n \rightarrow \infty} \left(1 - \frac{f}{n\langle f_s \rangle}\right)^{n-2} = e^{-f/\langle f_s \rangle}. \quad (3)$$

We see that in this limit anisotropy induces an exponential tail in $P(f)$. We next investigate the extent to which the limiting behavior is reflected at finite anisotropies.

To gain some intuition for the approach to the anisotropic limit we return to the 3×3 case, which can be solved analytically. We let $P_s(f)$ and $P_w(f)$ denote the separate distributions of forces in the strong and weak directions, respectively. $P_w(f)$ is identical to $P(f)$ in Eqn. 3. In the strong direction, however, the situation is more complicated. A complete expression is given in Appendix C.

For the 3×3 case, the fully anisotropic limit $\alpha \rightarrow \infty$ has $P(f) = \frac{2}{9}\langle f_s \rangle^{-2}(3\langle f_s \rangle - f)$, $f \in [0, 3\langle f_s \rangle]$, a piecewise linear function. For $\alpha > 2$, $P(f)$ is given by $P_s^{(2b)}(f)$ (from Appendix C) between F and Δ . $P_s^{(2b)}$ is a linear function, and the interval from F to Δ grows with α . As

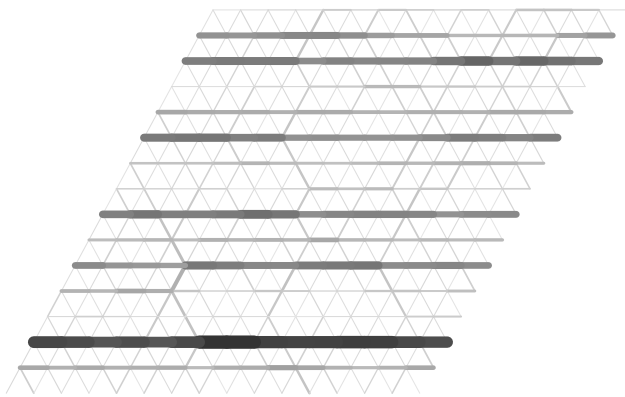


FIG. 14: A 15×15 anisotropic lattice with $\alpha = 5$. The force on an edge is redundantly mapped to color and width (stronger forces are darker and thicker). The stronger stress is imposed in the horizontal direction.

α increases further the width of this region grows and the slope approaches the limiting slope of $-\frac{2}{9}\langle f_s \rangle^{-2}$. $P_s(f)$ is plotted for increasing α in Fig. 13.

On larger lattices, numerical calculations show similar behavior to the 3×3 case, but with the limiting linear distribution replaced by the limiting exponential of the large system limit over the range of forces of interest. (The distribution must be cut off at $f = F_s$.) Fig. 14 shows a typical anisotropic configuration. Fig. 15 shows $P(f)$ for anisotropic lattice of size 15×15 , with the contributions from the weak and strong directions shown separately. The role of the strong direction in broadening the distribution is clear. Results are shown for two cases, one in which strong forces are imposed on a single lattice direction and another in which strong forces are imposed on two lattice directions. Note the difference in behavior for small f . In the latter case there is no peak in $P(f)$ for small f .

Fig. 16 shows force distributions on a 15×15 lattice for several values of α . For sufficiently large α a middle portion of $P(f)$ appears to be exponential. As α increases, so does the extent of this portion. We hold $\langle f_s \rangle$ fixed so that every curve will have the same decay length.

We conclude that $P(f)$ on the anisotropic lattice displays an exponential tail in the following sense. For moderate α and n , a portion of the tail of $P(f)$ is nearly linear on a log plot. The decay is not truly exponential because of the finite anisotropy and finite lattice size, but the limiting behavior of $P(f)$ as n and α are increased is a true exponential. The region of nearly exponential decay grows with increasing anisotropy, extending as far as $f \approx 3\langle f_s \rangle$ for $\alpha = 8$.

We note that the parameter α can be related to the angle of internal friction in the following way. The ratio of major and minor principal stresses is $\sigma_1/\sigma_2 = (\alpha + 1)/\sqrt{3}$. By exploiting the relation $\sigma_1/\sigma_2 = (1 + \sin \phi)/(1 - \sin \phi)$ [24], where ϕ is the angle of internal friction, we find that $\alpha = 8$ corresponds to an internal friction of approx-

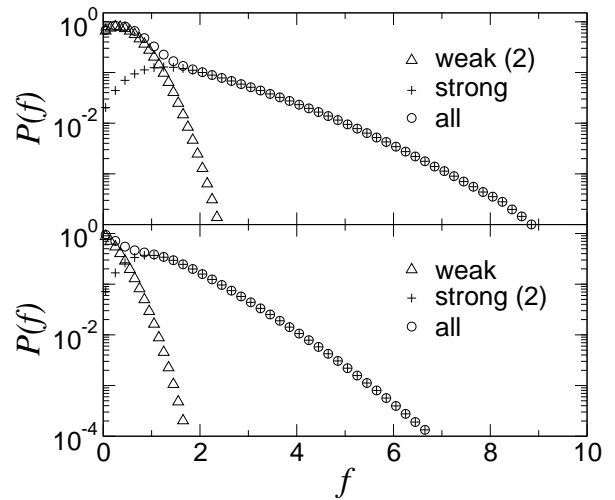


FIG. 15: $P(f)$ for strong, weak, and all lattice directions on a 15×15 lattice with $\alpha = 3$. The strong direction(s) is entirely responsible for the tail in $P(f)$. Top: Two weak F_k 's and one strong. Bottom: One weak F_k and two strong. On both plots, $\langle f \rangle = 1$.

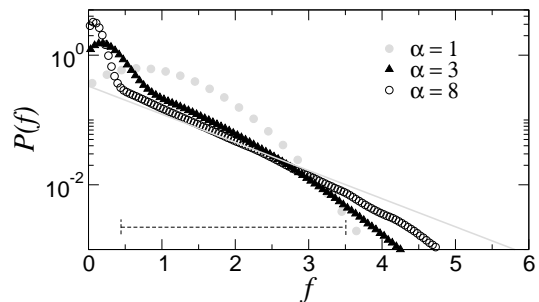


FIG. 16: $P(f)$ on a 15×15 lattice for increasing anisotropy. Portions of the tail for stronger anisotropies are difficult to distinguish from exponential decay, and the limiting behavior is a true exponential (gray line). The dashed line indicates the interval in f over which the $\alpha = 8$ curve is approximately exponential. $\langle f_s \rangle = 1$ for every curve.

imately 43° .

The survival of the exponential tail of strong forces in large triangular lattices under anisotropic loading can be traced to the discussion based on Fig. 2 concerning the sums of forces along layers of edges in the various directions. That argument shows that the strong forces in one lattice direction cannot be redistributed into the other directions due to vector force balance constraints. Thus for strongly anisotropic lattices, the strong forces will follow scaling laws close to the limiting exponential form corresponding to no force at all in the weak direction(s). Note that in the case of two strong directions and one weak, the two strong are effectively independent since strong chains from the two directions cannot interact significantly without generating a strong chain in the supposedly weak direction and thereby reducing the degree of anisotropy.

VI. CONCLUSION

We have investigated the distribution $P(f)$ of contact forces on a lattice of triangular bonds under the Edwards flat measure. An interesting question is whether one expects exponential decay in $P(f)$. The triangular lattice is a simple but nontrivial system for studying this phenomenon.

The distribution on the $n \times n$ periodic lattice decays faster than exponentially, as reported previously.[14] Diluting the lattice induces significant broadening in $P(f)$, but the decay remains faster than exponential. Even at rigidity percolation associated with random bond dilution of the lattice, no qualitative change in the form of $P(f)$ is discernible. In particular, we do not see evidence for an exponential tail associated with the transition. This is related to the fact that the transition is first order.

On the other hand, imposing anisotropic stress on the undiluted lattice can induce an exponential tail in $P(f)$. In the limit of an infinite lattice with stress imposed only along one lattice direction, the distribution of contact forces is a pure exponential. Numerical simulation shows that evidence of this behavior may still be seen for finite lattice sizes and a finite ratio of the compressive forces in the strong and weak directions. In such a scenario the tail of $P(f)$ is not a true exponential, but appears approximately linear on a log plot of $P(f)$ for some interval in f . For large enough anisotropies, $P(f)$ decays three orders of magnitude from its maximum and $f \approx 3\langle f_s \rangle$ before deviation from exponential decay becomes obvious.

In the triangular lattice model, anisotropy is associated with the appearance of long force chains oriented along the strong direction, a phenomenon that has also been observed in experiments.[25, 26]

Acknowledgments

We thank R. Wolpert, B. Rider and R. Connelly for helpful conversations. This work was supported by NSF grant DMR-01-37119.

APPENDIX A: ANALYTIC $P(f)$

$P(f)$ for the 3×3 isotropic lattice is calculated as follows. There are $3^2 - 1 = 8$ degrees of freedom; we take nine basis elements subject to a constraint which is to be imposed by hand. Three of these elements are shown in Fig. 17. There are three honeycomb elements, ϕ_i , $i = 1 \dots 3$, three elements ψ_{j1} , $j = 1 \dots 3$, and three elements ψ_{j2} . The figure depicts ϕ_1 , ψ_{11} , and ψ_{12} . The ψ elements make no net contribution to the total force in the system. The three ϕ elements must sum to F ; this is the additional constraint we impose. All elements are isotropic by construction.

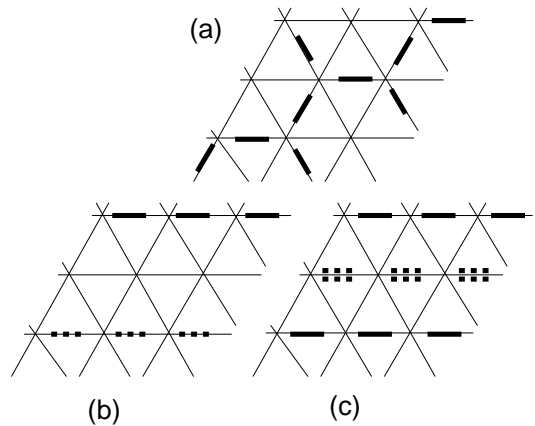


FIG. 17: Three of the nine basis elements employed to evaluate Eqn. 1 for the 3×3 isotropic lattice. Solid bars indicate a positive contribution to the force on an edge; dashed bars indicate a negative contribution. Double bars indicate a contribution with twice the weight. The honeycomb in (a) is one of three. The elements in (b) and (c) are each repeated for the other two lattice directions.

Eqn. 1 can be rewritten

$$P(f) = \frac{1}{N} \prod_{i=1}^3 \int_0^F d\phi_i \prod_{j=1}^3 \int_{\phi_0/2}^{\phi_0} d\psi_{j2} \int_{-\phi_0+\psi_{j2}}^{\phi_0-\psi_{j2}} d\psi_{j1} \times \delta(f - (\phi_1 - 2\psi_{12})) \times \delta(\phi_1 + \phi_2 + \phi_3 - F) \quad (A1)$$

where $\phi_0 = \min(\{\phi_1, \phi_2, \phi_3\})$. The first δ -function fixes a particular edge to support force f ; all edges are equivalent by symmetry. The bounds on the ψ 's assure that no edge will support tensile force. The presence of ϕ_0 breaks the integral into three regions. The regions wherein $\phi_0 = \phi_2$ and $\phi_0 = \phi_3$ are identical; the region where $\phi_0 = \phi_1$ must be evaluated separately because ϕ_1 touches the edge fixed to carry f .

The evaluated expression is given in Eqn. 3.

APPENDIX B: PROOF THERE ARE $n^2 - 1$ INDEPENDENT WHEEL MOVES

Designate a linear combination of wheel moves by an n^2 -dimensional vector of coefficients z_i and call the corresponding move Z . With each node, we associate a three-dimensional position \vec{x}_i , where the first two components represent its position in the plane and the third is z_i . Consider the wheel moves centered on any three nodes that form a unit triangle and let the 3D points associated with these nodes be \vec{x}_1 , \vec{x}_2 , and \vec{x}_3 . These points define a plane Y in the 3D space. Now consider the edge between nodes 1 and 2. Define node 4 to be the reflection of node 3 through that edge. If the edge in question is to remain unchanged under the action of Z , we must have $z_1 + z_2 - z_3 - z_4 = 0$, since the edge is on the spokes of nodes 1 and 2 and the rim of 3 and 4. This value of z_4 is

precisely the value that places \vec{x}_4 in the plane Y , as can easily be confirmed by writing the equation for the plane and noting that, for any rhombus where points 3 and 4 are at opposite ends of a diagonal, $x_1 + x_2 - x_3 - x_4 = 0$. Extending this reasoning to additional nodes we see that all of the vectors \vec{x}_i must lie in the same plane Y if Z is to generate no changes on any of the edges. There is only one way, however, that Y can be oriented so as to satisfy the periodic boundary conditions on the lattice: Y must be horizontal, corresponding to the linear combination in which all wheel moves have equal weight. QED

APPENDIX C: ANISOTROPIC $P(f)$ ON THE 3×3 LATTICE

The calculation of $P(f)$ for the anisotropic 3×3 case proceeds similarly to the isotropic calculation. The

anisotropy requires the division of the relevant integral according to whether the force f is greater than or less than the difference Δ between the strong F_i and the weak ones. For the case $\Delta < F$, we find

$$P_s(f) = \frac{1}{N} \begin{cases} P_s^{(1)}(f) & f < \Delta \\ P_s^{(2a)}(f) & \Delta < f < F \\ P_s^{(3)}(f) & F < f < F + \Delta, \end{cases} \quad (C1)$$

where V is a normalization constant and the P_s 's are given below. For the case $\Delta > F$

$$P_s(f) = \frac{1}{N} \begin{cases} P_s^{(1)}(f) & f < F \\ P_s^{(2b)}(f) & F < f < \Delta \\ P_s^{(3)}(f) & \Delta < f < F + \Delta. \end{cases} \quad (C2)$$

The functions P_s in Eqn. C2 are

$$P_s^{(1)}(f) = (7\alpha - 2)F^7 + 21(4\alpha - 1)F^6f - 42(5\alpha + 1)F^5f^2 + 140(2\alpha + 1)F^4f^3 - 210(\alpha + 1)F^3f^4 + 84(\alpha + 2)F^2f^5 - 14(\alpha + 5)Ff^6 + 12f^7; \quad (C3)$$

$$P_s^{(2a)}(f) = (3\alpha^7 - 14\alpha^6 + 21\alpha^5 - 35\alpha^3 + 42\alpha^2 - 14\alpha + 2)F^7 + 21(\alpha^4 - 4\alpha^3 + 5\alpha^2 - 5)\alpha^2F^6f + 21(3\alpha^4 - 10\alpha^3 + 10\alpha^2 - 15)\alpha F^5f^2 - 35(3\alpha^4 - 8\alpha^3 + 6\alpha^2 - 8\alpha - 5)F^4f^3 + 105(\alpha^3 - 2\alpha^2 - \alpha - 2)F^3f^4 - 21(3\alpha^2 - 8\alpha - 7)F^2f^5 + 7(\alpha - 12)Ff^6 + 9f^7; \quad (C4)$$

$$P_s^{(2b)}(f) = (21\alpha - 4)F^7 - 21F^6f; \quad (C5)$$

$$P_s^{(3)}(f) = (\alpha F - f)^2 [(-3\alpha^5 - 14\alpha^4 - 21\alpha^3 + 35\alpha - 42)F^5 + (15\alpha^4 - 56\alpha^3 + 63\alpha^2 - 35)F^4f + (30\alpha^2 - 56\alpha + 21)F^2f^3 - 3(10\alpha^2 - 28\alpha + 21)\alpha F^3f^2 - (15\alpha - 14)Ff^4 + 3f^5]. \quad (C6)$$

-
- [1] T. G. Drake, J. of Geophysical Research **95**, 8681 (1990).
 - [2] M. Babić, in *Advances in Micromechanics of Granular Materials*, edited by H.H. Sheen et al. (Elsevier Science Publisher, Amsterdam, 1992), p. 291.
 - [3] P. Deltour and J.-L. Barrat, J. Phys. I France **7**, 137 (1997).
 - [4] S. T. Thoroddsen and A. Q. Shen, Physics of Fluids **13** (1), 4 (2001).
 - [5] D. Lohse, R. Bergmann, R. Mikkelsen, and et al., Phys. Rev. Lett. **93**, 198003 (2005).
 - [6] P. Dantu, Ann. Ponts Chauss. **IV**, 193 (1967).
 - [7] S. R. Nagel, Rev. of Mod. Phys. **64**, 321 (1992).
 - [8] P. Claudin, Master's thesis, University of Cambridge (1995).
 - [9] F. Radjai and S. Roux, Phys. Rev. Lett. **89**, 064302 (2002).
 - [10] D. L. B. et al., Phys. Rev. E **63**, 041204 (2001).
 - [11] G. Løvøll, K. J. Måløy, and E. G. Flekkøy, Phys. Rev. E **60**, 5872 (1999).
 - [12] D. M. Mueth, H. M. Jaeger, and S. R. Nagel, Phys. Rev. E **57**, 3164 (1998).
 - [13] S. N. Coppersmith, C. Liu, S. Majumdar, O. Narayan, and T. A. Witten, Phys. Rev. E **53**, 4673 (1996).
 - [14] J. H. Snoeijer, T. J. H. Vlugt, M. van Hecke, and W. van Saarloos, Phys. Rev. Lett. **92**, 054302 (2004).
 - [15] J. Snoeijer, T. J. H. Vlugt, W. G. Ellenbroek, and M. van Hecke J. M. J. van Leeuwen, Phys. Rev. E **70**, 061306 (2004).
 - [16] J. E. S. Socolar, Phys. Rev. E **57**, 3204 (1998).
 - [17] S. F. Edwards and D. V. Grinev, *Statistical mechanics of granular materials: stress propagation and distribution of contact forces* (Springer-Verlag, 2003), pp. 147–153.
 - [18] A. V. Tkachenko and T. A. Witten, Phys. Rev. E **62**, 2510 (2000).
 - [19] S. F. Edwards, in *Granular Matter: An Interdisciplinary Approach*, edited by A. Mehta (Springer, New York, 1994), pp. 121–140.
 - [20] W. H. Press, S. A. Teukolsky, W. T. Vetterling, , and B. P. Flannery, *Simulated Annealing Methods* (Cambridge University Press, 1992), pp. 444–455.
 - [21] R. Durrett, *Probability: Theory and Examples* (Thomson Books/Cole, 2005), chap. 5.

- [22] R. Connelly, K. Rybnikov, and S. Volkov, J. Stat. Phys. **105**, 143 (2001).
- [23] W. H. Press, S. A. Teukolsky, W. T. Vetterling, and B. P. Flannery, *Linear Programming and the Simplex Method* (Cambridge University Press, 1992), pp. 430–443.
- [24] R. M. Nedderman, *Statics and kinematics of granular materials* (Cambr. Univ. Press, Cambridge, 1992).
- [25] T. S. Majmudar and R. P. Behringer, submitted to Nature (2005).
- [26] B. Utter and R. P. Behringer, Euro. Phys. J. E **14**, 373 (2004).